DATA REPOSITORY MATERIAL FOR

Deformation of Gondwana Margin Turbidites during the Pampean Orogeny, North-central Argentina

Detailed Structural Data

The locations for the data from the three areas, northern, transitional, and southern, are keyed to Fig. 1 of the main paper.

Northern sections

The Puncoviscana Formation (*sensu stricto*) in northern sections (the highest structural level) consists of a turbiditic sequence of 5 to 15 cm-thick greywacke beds alternating with 3 to 10 cm-thick shaly layers. Sedimentary structures, such as parallel- and cross-bedding, and flame structures are locally preserved in sandier layers. A weak, compaction-related, bedding-parallel cleavage (S_c) occurs in greywacke and shale beds, but is better-developed in shales and pelites. In addition to S_c, a disjunctive fanning tectonic cleavage (S_1) that is developed in pelites and locally observed as a flow cleavage, is associated with ubiquitous meter- to decameter-scale, upright chevron folds (F_1) that have gentle N or NE plunges (Fig. DR1). These chevron folds are characteristic of all northern sections. Locally, chevron folds have less than 60º interlimb angles, saddle reefs, and hinge collapse structures. S_1 planes have approximately 1cm spacing and generally intersect S_0 and S_c at 10 to 15°. Younger meter- to decameter-scale, open to gentle folds (F_{1a}) are characterized by rounded hinges, and sub-horizontal NNE-SSW axes. F_{1a} folds are coaxial with F_1 and have no associated cleavage; their axial planes are sub-horizontal to subvertical, and dip to both east and west.

A variably developed, bedding-parallel, compaction cleavage (S_c) is defined in shaly beds of the northern area by aligned detrital micas, pressure solution seams, and elongated quartz grains that are internally strain free (Fig. DR2a). The quartz grains have curved grain boundaries (Fig. DR2a) and pressure shadows consistent with pressure solution as the principal mechanism for shape change. A few large chlorite-mica stacks and detrital chlorite grains are kinked or oblique to the main cleavage (Fig. DR2a) and

exhibit pressure shadows in which fine-grained chlorite and/or quartz has precipitated. Greywackes contain discontinuous mica seams that are longer than individual quartz clasts and a locally well-defined grain alignment fabric (S_c) that is bedding-parallel. Mica beards on clasts are aligned parallel to quartz grain long axes (Fig. DR2b) and stylolites sub-parallel to S_0 have also been observed. Evidence of shearing on fold limbs is given by asymmetrical quartz grains and pressure shadows, and dissolved borders on quartz and mica grains.

Middle (transitional) sections

The Hualinchay, Choromoro, Vipos, and Siambon sections (Fig. 1) contain up to 70 cm-thick alternations of psammitic and pelitic beds. Sedimentary structures (cross- and parallel-bedding) are well-preserved in psammitic layers. Pelites have a well-developed and continuous compaction-related (S_c) cleavage that is parallel or subparallel to S_0, and a spaced, fanning S_1 cleavage associated with meter-scale chevron F_1 folds. S_1 intersects S_0 and S_c at 15-20° angles in chevron fold limbs. In psammites, S_1 is a widely-spaced rough cleavage (~1-2 cm spacing), that locally intersects S_c (and S_0) and becomes progressively more pervasive and better-defined southwards. This regularly spaced S_1 cleavage is highly characteristic of outcrops throughout the transitional zone. In most outcrops, axial planes of close F_1 folds dip steeply to the west; sub-horizontal F_1 axes and parallel S_0/S_1 intersection lineations generally trend NNE-SSW (Fig. DR3). Extension gashes, often filled with quartz fibers, are common in fold limbs. Collapse hinge structures are also common. In Siambon, mm- to cm-scale parasitic F_1 folds are also observed.

Concentric, open to gentle, cm- to m-scale F_{1a} folds are generally coaxial with F_1, but their axes are more variable in orientation than those of F_1 axes (Fig. DR3) and axial planes generally range from sub-horizontal to NE or NW steeply-dipping. Although there is an associated crenulation, no new mica growth is observed. Striations perpendicular to F_{1a} axes are common. F_1-related quartz-filled extension gashes are offset by bedding plane slip on F_{1a} fold limbs. We group these folds with F_{1a} elsewhere in the region.

To the east of Cumbres Calchaquies, in the Sierra del Nogalito (Fig. 1), there is a monotonous and tightly chevron-folded (F_1) sequence of phyllites and biotite schists. Millimeter-scale, bedding-parallel banding (S_c) strikes NE, and dips steeply to the NW (Fig. DR3). Thin (2–3mm) quartzitic layers alternate with 0.5–2mm-thick micaceous layers; no unambiguous sedimentary structures have been observed. Centimeter-scale chevron folds (F_1) have NE-SW trending axes and axial planes dipping to the NW (Fig. DR3). In southern and more quartzitic localities of the Sierra del Nogalito, F_1 folds are scarce.

In weakly metamorphosed pelites, a well-defined bedding-parallel fabric (S_c) is defined by aligned, fine-grained detrital micas (Fig. DR2c). At progressively higher metamorphic grade, to the south, an increasing number of larger muscovite grains (100-150 μm) define S_c. Symmetric quartz and feldspar grains have dissolved, curved borders with thin layers of oxide deposits and a well-developed shape-preferred orientation parallel to S_c (Fig. DR2c). A superposed anastomosing tectonic cleavage, S_1, is defined by the alignment of new (50-100 μm) mica and chlorite grains oblique to S_0 and S_c (Fig. DR2d) and by asymmetrically dissolved quartz grains with pressure shadows that contain fine-grained recrystallized quartz and chlorite.

Psammitic rocks derived from greywackes almost always contain 1 to 2 cm-thick quartz-rich lithons separated by distinctive, anastomosing 0.5–3 mm-thick mica-rich cleavage domains (S_c) that are parallel or subparallel to S_0. Locally, grain size gradation (Fig. DR2d) and cross stratification are preserved. In the lithons, sub-rounded to angular quartz and feldspar clasts have locally interpenetrating grain boundaries and a well-developed shape-preferred orientation (S_c) parallel to S_0 (Fig. DR2e). Mica beards and asymmetric quartz and feldspar grains are common on fold limbs (Fig. DR2e). Isolated muscovite grains or thin mica-film segments define a weak, superimposed sigmoidal cleavage (S_1) at approximately 45° to S_c (Fig. DR2e). The mica-rich S_c cleavage zones contain oxide-rich pressure solution seams and films of fine-grained tabular muscovites and chlorites that wrap around truncated quartz and feldspar clasts. Dissolved quartz grain borders and accumulation of oxides indicate that pressure solution was an important mechanism for both, the development of S_c and S_1 in these rocks. A younger crenulation (F_{1a}), affects pelitic and psammitic layers without the formation of new micas.

In the Nogalito area (Fig. 1), where metamorphism in the tightly chevron-folded schists reached biotite grade, S_c is defined by alternating 2–3 mm-thick quartz-rich lithons and 1 mm-thick mica-rich seams. Although the geometry of the regularly spaced S_c cleavage domains locally has the superficial appearance of sedimentary cross-stratification seen elsewhere in middle sections, the quartzitic lithons are here almost completely recrystallized and there is no evidence for graded bedding. On the limbs of cm-scale chevron folds, quartz and feldspar grains have a strong preferred shape orientation that is both parallel and oblique to layering (S_c and S_1, respectively), whereas in the chevron hinges, there is no axial plane cleavage visible and grains are equant, although relicts of an S_c defined by corroded biotites are still preserved. Quartz and feldspar grains have interpenetrating borders and most contain deformation bands and evidence for grain boundary migration. Mica-films within lithons are generally parallel to the long axis of quartz grains and contain mostly fibrous, pale biotite with lesser amounts of muscovite, which is more abundant in fold limbs than in hinges. On fold limbs, the mica seams contain large asymmetrical quartz and feldspar grains with dissolved borders and pressure shadows, and abundant pressure-solution seams. Tabular and well-developed muscovite, oriented parallel to the limbs of chevron folds, overgrows the biotites. Deformation twins in plagioclase grains, mechanical flexion of large (metamorphic) muscovites, and transgranular fractures are likely related to the younger, brittle folding episode (F_2).

Southern sections

To the south, recognizable psammites and pelites gradually change into banded schists and gneisses with a pervasive compositional banding. There are no preserved sedimentary structures. Close, decimeter to meter-scale harmonic chevron folds (F_1) have sub-horizontal to moderately SE-plunging axes (Fig. DR4) and axial planes that dip to the NE. Asymmetric F_1 parasitic folds are common, in contrast to northern areas where chevron folds have straight limbs, except where affected by F_{1a}. Axis-parallel mineral and intersection lineations (L_1) plunge gently to SE. Occasional folded quartz veins have axial planes sub-parallel to the tectonic banding and 1–3 cm-thick calc-silicate veins

obliquely cut S_1. Post-tectonic andalusite, garnet, and staurolite porphyroblasts occur adjacent to Ordovician plutons (see also Toselli & Rossi de Toselli, 1984).

In the Sierra de Ambato area (Fig. 1), pelitic and psammitic schists that have a distinctive compositional banding are also affected by close, cm- to meter-scale F_1 folds with an associated fanning cleavage S_1 that strikes predominantly NNW-SSE and dips steeply to the WSW; F_1 axes and an associated crenulation lineation (L_1) plunge gently to the SE (Fig. DR4). Locally, mm-scale, post-S_1 garnet porphyroblasts are observed and cm-thick pegmatite veins profusely intrude the sequence, cross-cutting S_1 at high angles. Shear bands of 0.5 to 1 m width, related to slip between layers during chevron folding, are common in F_1 limbs and also affect the pegmatites.

The El Jumeal and Ancasti Formation rocks of the Sierra de Ancasti (Fig. 1; Willner, 1983; Willner & Miller, 1982) have a compositional banding that these authors interpret as S_1 and which strikes NNW and dips steeply to NNE or SSW (Fig. DR4). Close F_1 folds have axial plane foliations and sub-vertical to steeply NE-dipping axial planes. Asymmetrical parasitic folds are common and most fold axes and associated lineations plunge moderately to the NNW, less commonly to the SSE (Fig. DR4), except adjacent to Ordovician plutons, where the scatter of orientation is high.

In banded schists of southern sections, S_c is a well-developed solution cleavage and with increase in metamorphic temperature, there is an increase in quartz-vein segregations subparallel to S_0. Locally, these rocks underwent a regionally important post-tectonic (i.e., post F_1) static metamorphic event that led to intense recrystallization of the sequence and porphyroblast growth (Toselli 1990; Toselli & Rossi de Toselli, 1990). In thin section, equant, polygonal quartz and plagioclase grains exhibit curved or straight borders and triple points. Despite this annealing overprint, it is still possible to identify at least two pre-annealing fabrics: an early-formed compositional banding (that is, S_0/S_c) on fold limbs, and a later S_1 that is axial planar to F_1 folds (Fig. DR2f). Early-formed S_c is defined by alternating quartz-rich bands and bands of large corroded biotite grains that are kinked or show other signs of internal deformation such as micro-folding. S_1 is defined by aligned, mm-scale euhedral biotite grains (Fig. DR2f). Post-tectonic

garnet porphyroblasts (1-2 mm diameter) do not contain inclusion trails, have no strain shadows, and none of the foliations present in the rock wraps around them (Fig. DR2f).

Figure DR1. Simplified geological map of northern sections (Fig. 1b) with structural data plotted on lower hemisphere stereographic projections. Number of structural data (stereoplot number between brackets): Tilcara (1) S_0 n=149, S_1 n=67; Cuevas (2) S_0 n=18, S_1 n=18, F_1 axes n=7; Quebrada del Toro (3) S_0 n= 49, S_1 n=17, F_1 axes n=16, F_{1a} axes n=18.

Figure DR2. Photomicrographs of S_c and S_1 in shale and sandstone from Quebrada del Toro and Quebrada de Don Bartolo (Fig. 1b) and from pelites and psammites from Choromoro and Hualinchay sections (Fig. 1). a) Q. del Toro pelite: S_c defined by orientation of detrital micas and chlorite. Interspersed are quartz grains (long arrow) with dissolved borders and chlorite grains sub-perpendicular to S_c with asymmetric pressure shadows (short arrows). b) Q. de Don Bartolo sandstone: Micabeards (arrowed) on quartz (Q) and feldspar (F) clasts. c) Choromoro pelite: S_c defined by quartz, chlorite, and white mica grains. S_1 defined by white mica only. d) Hualinchay section: Primary (S_0) contact of pelitic (upper) and psammitic (lower) beds subparallel to S_c. Weakly anastomosing S_1 defined by white micas and elongate quartz. Vertical arrow shows grain size gradation. e) Hualinchay psammite: S_c defined by preferred alignment of symmetric and asymmetric dissolved quartz grains (some with interpenetrated borders; short arrows), muscovite (M), and mica beards on quartz clasts (long arrow). f) Compositional banding (S_c) and axial plane foliation (S_1, defined by biotites). Post-tectonic garnet (G) crosscuts the compositional banding and S_1. Quartz annealing occurred during Ordovician contact metamorphism.

Figure DR3. Simplified geological map of middle sections and Tafi (Fig. 1b). Legend for map and stereographic projections as in Figure DR1. Number of structural data (stereoplot number between brackets): Hualinchay (4) S_0 n=163, S_1 n=24, F_1 axes n=15, F_{1a} n=62; Choromoro (5) S_0 n=78, S_1 n=15, F_1 axes n=8, F_{1a} n=4; Nogalito (6) S_0 n=27, F_1 axes n=16, F_2 n=13; Vipos (7) S_0 n=61, S_1 n=30, F_1 axes n=5, F_{1a} n=4; Siambón (8) S_0 n=51, S_1 n=9, F_1 axes n=4, F_{1a} n=15; Tafí (9) S_0 n=46, S_1 n=11, F_1 axes n=17, F_{1a} n=3.

Figure DR4. Simplified geological map of southern sections (Fig. 1b). Legend for map and stereographic projections as in Figure DR1. Number of structural data (stereoplot number between brackets): S. Fernando (10) S_0 n=10, S_1 n=6, F_1 axes n=21; N. Ancasti (11) S_0 n=22, S_1 n=3, F_1 axes n=15.

Figure DR5. Sequence of geologic events observed in the Northern, Eastern and Southern Sierras Pampeanas. Data for San Lorenzo Volcanic Complex and Alto de las Salinas Complex from: Gonzalez et al., 2000. Data for Salta Group from: Del Papa and Salfity, 1999. Data for all other events from citations in the text.

REFERENCES

Toselli, A., 1990, Metamorfismo del Ciclo Pampeano, *in* Aceñolaza, F.G., Miller, H. and Toselli, A.J., eds., El Ciclo Pampeano en el Noroeste Argentino: San Miguel de Tucumán, Universidad Nacional de Tucumán, v. 4, p. 181-197.

Toselli, A., and Rossi de Toselli, J. N., 1984, Metamorfismo de las Cumbres Calchaquíes: II Petrología del basamento esquistoso entre La Angostura y Tafí del Valle, Tucumán: Revista de la Asociación Geológica Argentina, v. 39, p. 262-275.

Toselli, A., and Rossi de Toselli, J. N., 1990, Plutonismo en la Formación Puncoviscana, *in* Aceñolaza, F.G., Miller, H. and Toselli, A.J., eds., El Ciclo Pampeano en el Noroeste Argentino: San Miguel de Tucumán, Universidad Nacional de Tucumán, v. 4, p. 221-227.

Willner, A.P.,1983, Evolución tectónica, *in* Aceñolaza, F.G., Miller, H., Toselli, A., eds., La Geología de la Sierra de Ancasti: Munster, Munstersche Forschungen zur Geologie und Paleontologie, v. 59, p. 157-187.

Willner, A.P., and Miller, H., 1982, Poliphase metamorphism in the Sierra de Ancasti (Pampean Ranges, NW Argentina) and its relation to deformation, *in* Congreso Latinoamericano de Geología: Buenos Aires, v. 3, p. 441-455.

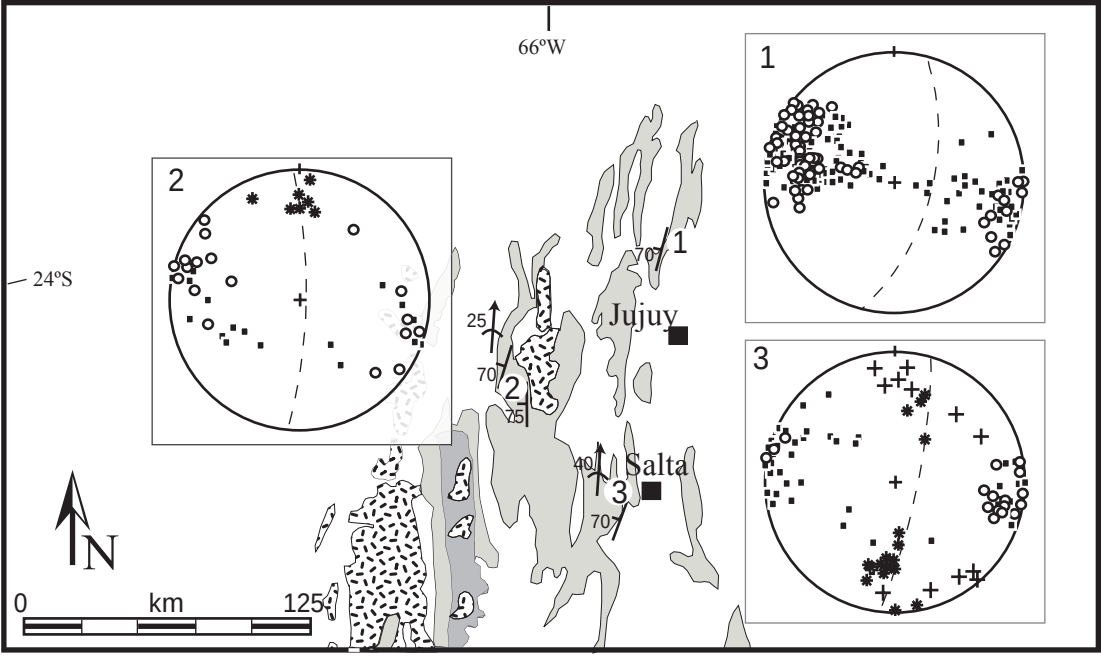

Map:

- Bedding (S_0)
- S_1
- F_1 axis
- F_{1a} axis
- F_2 (Andean axis)
- ① Region where structural data plotted
- Paleozoic intrusive and extrusive rocks
- High-grade metamorphic rocks
- Medium-grade metamorphic rocks
- Eocambrian Puncoviscana Fm.

Stereoplots:

- ■ poles to S_0 or S_c planes
- ○ poles to S_1 planes
- ✳ F_1 axis
- \+ F_{1a} axis
- △ F_2 axis

Dashed great circle: average S_0

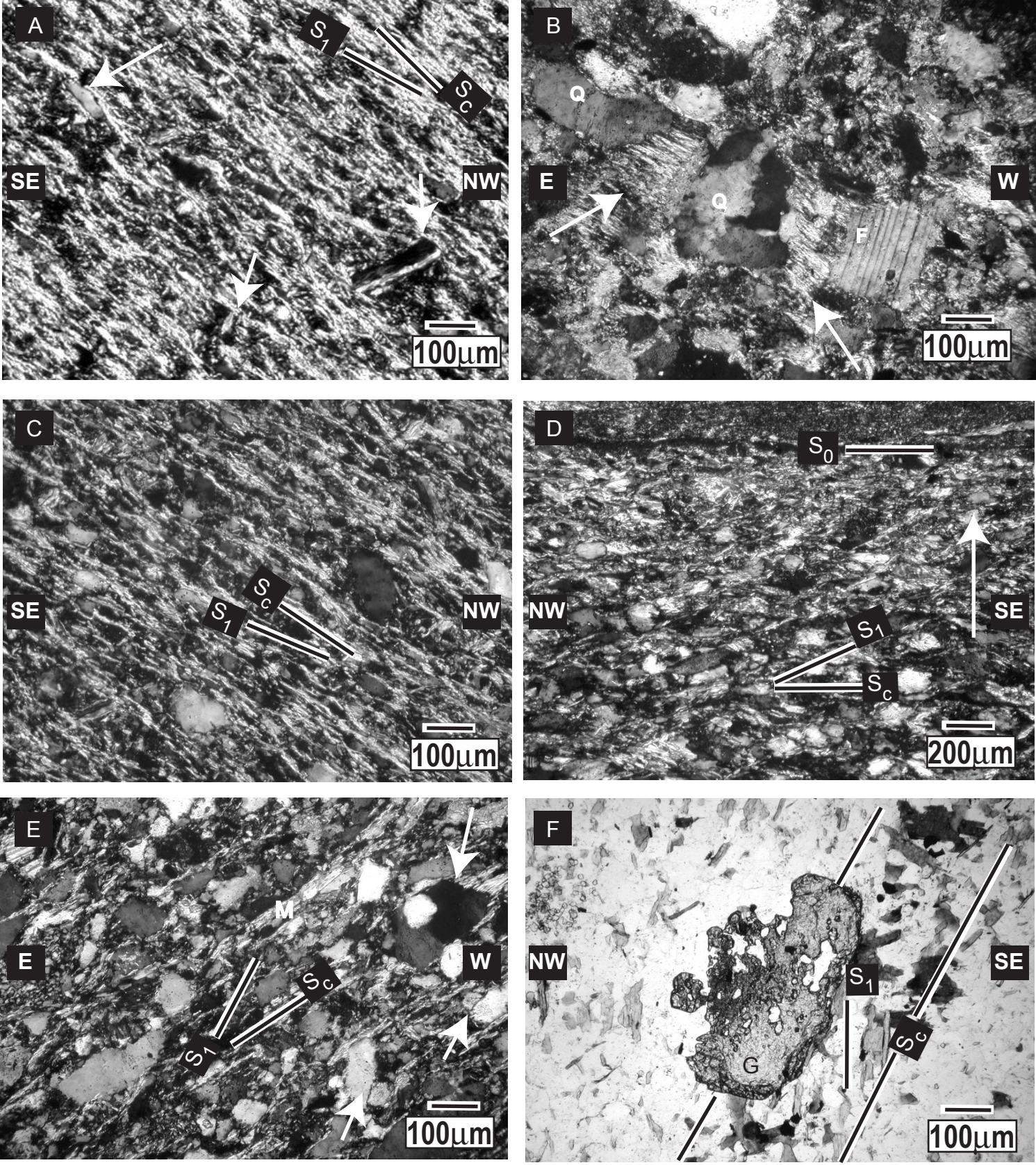
A
S_1
S_c
SE
NW
100μm
B
Q
E
Q
W
F
100μm
C
SE
S_c
S_1
NW
100μm
D
S_0
NW
SE
S_1
S_c
200μm
E
M
E
W
S_c
S_1
100μm
F
NW
S_1
SE
S_c
G
100μm

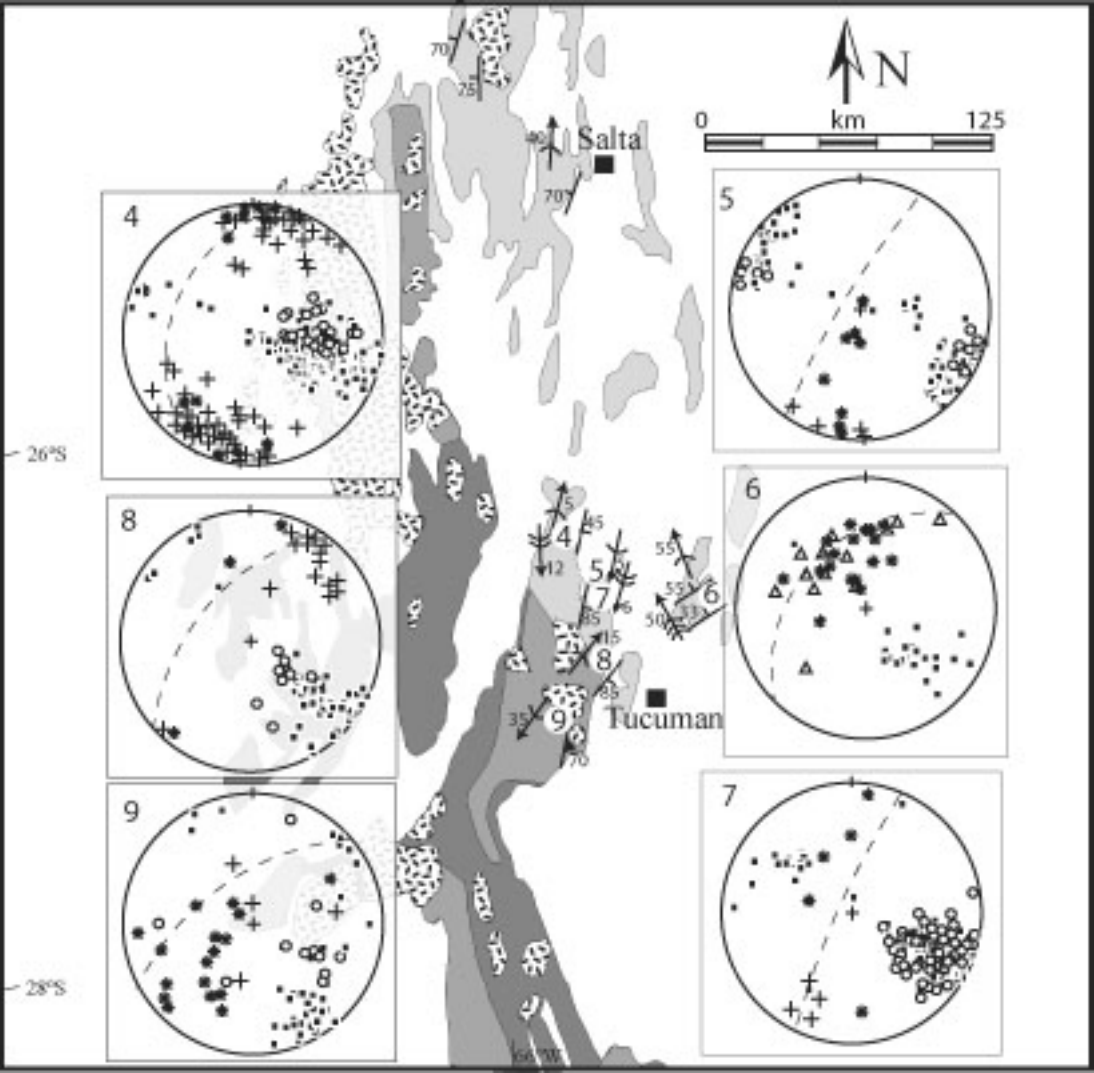
N
0
km
125
Salta
Tucuman
26°S
28°S
4
5
6
7
8
9

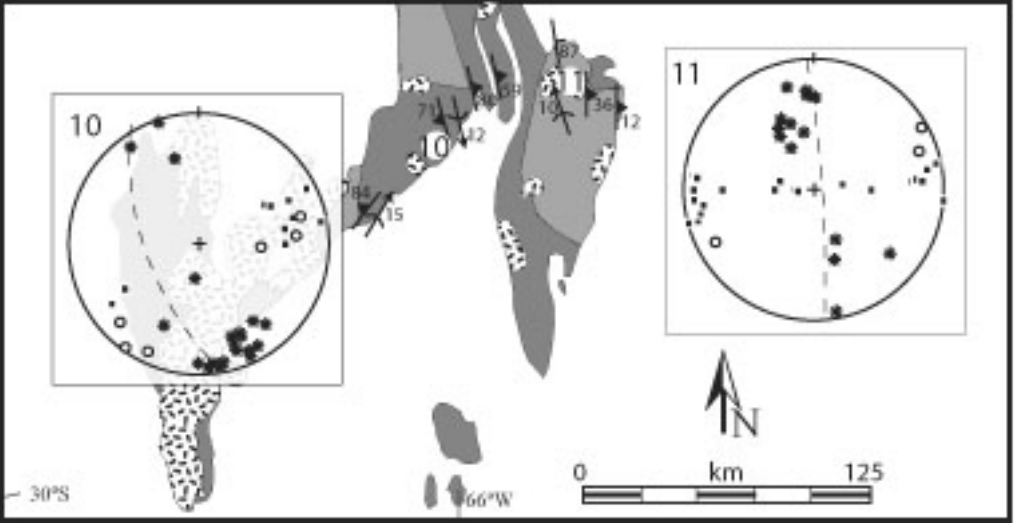
10
11
N
0
km
125
30°S
66°W

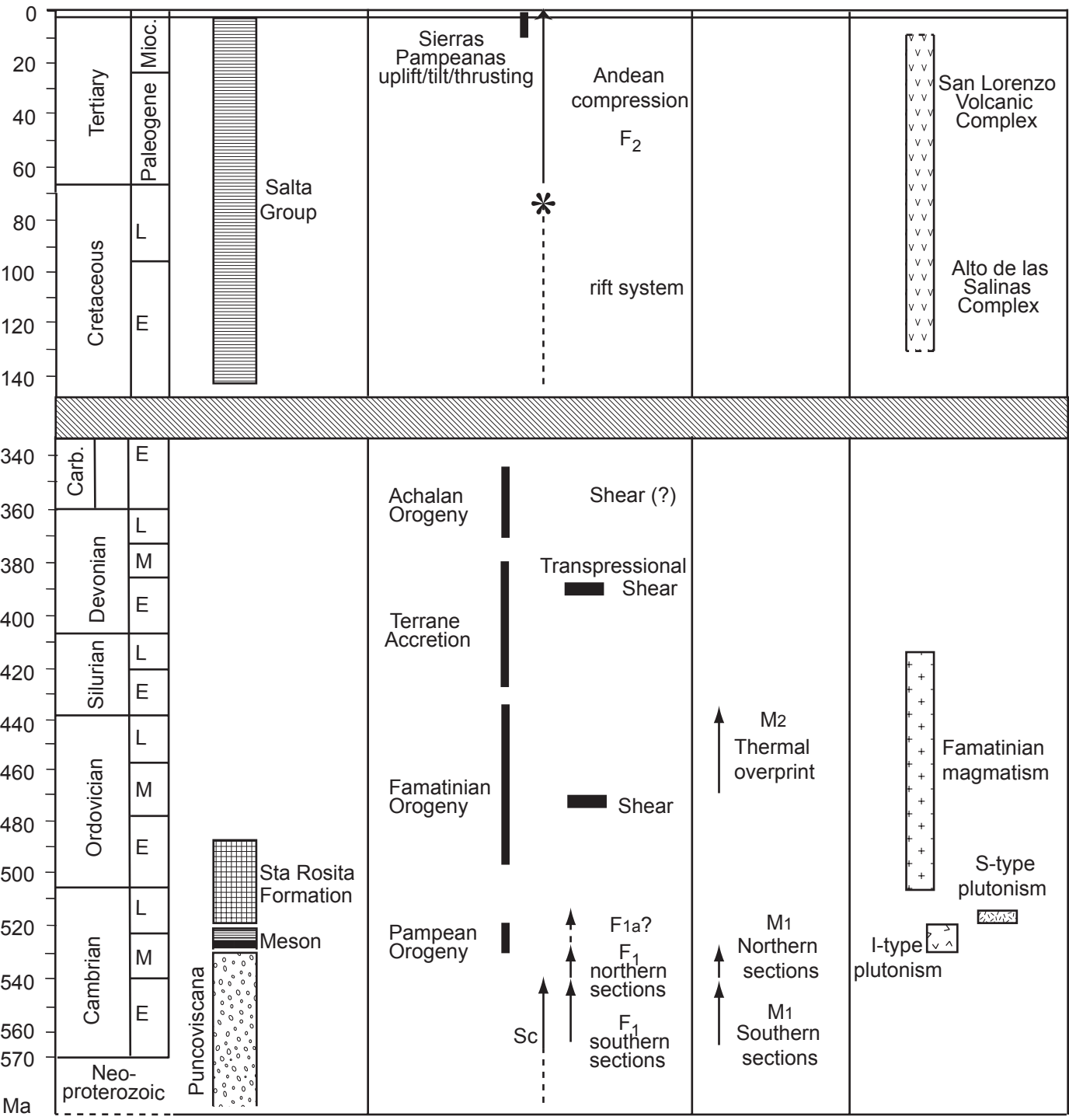
0
20
40
60
80
100
120
140
340
360
380
400
420
440
460
480
500
520
540
560
570
Ma
Tertiary
Mioc.
Paleogene
Cretaceous
L
E
Carb.
E
Devonian
L
M
E
Silurian
L
E
Ordovician
L
M
E
Cambrian
L
M
E
Neo-
proterozoic
Salta
Group
Sta Rosita
Formation
Meson
Puncoviscana
Sierras
Pampeanas
uplift/tilt/thrusting
Andean
compression
F2
rift system
Achalan
Orogeny
Shear (?)
Transpressional
Shear
Terrane
Accretion
Famatinian
Orogeny
Shear
Pampean
Orogeny
F1a?
F1
northern
sections
F1
southern
sections
Sc
M2
Thermal
overprint
M1
Northern
sections
M1
Southern
sections
San Lorenzo
Volcanic
Complex
Alto de las
Salinas
Complex
Famatinian
magmatism
S-type
plutonism
I-type
plutonism
Sedimentation
Deformation
Metamorphism
Magmatism